Research Article

Jun Liu*

Deep neural network application in real-time economic dispatch and frequency control of microgrids

https://doi.org/10.1515/nleng-2024-0074
received August 2, 2024; accepted October 24, 2024

Abstract: In recent years, the development of microgrids has driven the reform of the electricity market, breaking the monopoly of traditional power grids and promoting the healthy development of the electricity market. However, the stability of microgrids is significantly impacted by the integration of various energy sources and numerous users. This study explores the application of an intelligent dynamic programming algorithm based on the deep neural network algorithm, combined with adaptive dynamic programming. Subsequently, an intelligent real-time power generation control algorithm (IRPGC) is obtained by introducing rejection operation improvement. Finally, a real-time integrated scheduling and control framework for microgrids is constructed. The research results showed that the IRPGC algorithm had an average error of less than 10^{-5} after 5,000 iterations. Compared with mainstream algorithms, this algorithm achieved favorable results in frequency deviation evaluation indicators, with a frequency deviation fluctuation range of −0.073 to 0.013 Hz, an average error integral of 51.45, an absolute error integral of 0.54, and a time-weighted absolute error integral of 1.58×10^5. In the practical application of real-time microgrid power generation scheduling and control framework, the optimal rejection threshold range was found to be [0.94, 0.97]. The aforementioned results indicate that the proposed method exhibits good control performance and application effectiveness, providing a reference for real-time power generation scheduling and control in microgrids.

Keywords: deep neural network, microgrid, economic dispatch, frequency control, rejection operation

*** Corresponding author: Jun Liu,** Engineering Training Center, Shangluo University, Shangluo, 726000, China; Key Laboratory of Vanadium Battery Materials in Shaanxi Province's Higher Education Institutions, Shangluo University, Shangluo, 726000, China, e-mail: realliujun@163.com

1 Introduction

In recent years, with the rapid growth of renewable energy generation, the introduction of renewable energy, integration of emerging loads and power electronic devices, the source load fluctuations, and control complexity of microgrids have increased, posing severe challenges to the stability and safe operation of power systems [1–3]. In the future, developing comprehensive smart energy is one of the important directions to promote energy transformation, upgrading, and innovative development models. The development of comprehensive smart energy requires continuous innovation breakthroughs and policy support. From an economic perspective, the development of microgrids is currently facing enormous challenges. The parity of new energy on the grid does not necessarily mean parity utilization, which imposes a huge burden on the regulation costs of the power grid system. Meanwhile, only about 30% of low-carbon, zero-carbon, and negative-carbon technologies have entered commercial operation, making it very difficult or costly to regulate the power grid solely using advanced technologies. Yao and Sheng and Santra *et al.* found that as fossil fuels continue to pose serious threats to the global environment, new energy has attracted widespread attention from countries around the world due to its green and renewable advantages [4,5]. In the application of artificial intelligence technology in microgrids, deep neural network (DNN) algorithms have significant advantages. They can release the massive multisource data accumulated in the power system to greater value and quickly respond and adjust energy optimization management. Kumar *et al.* and Shakti *et al.* found that the DNN algorithms have strong data processing and prediction capabilities, as well as good flexibility, which are very suitable for different operating modes of microgrids. However, their computational complexity is high, and they are prone to problems such as overfitting and poor generalization ability [6,7]. To address these issues, this study combines the DNN algorithm with adaptive dynamic programming (ADP) to develop an intelligent

dynamic programming algorithm (DNN-ADP). Subsequently, the reject operation is performed to optimize the DNN-ADP algorithm, resulting in the intelligent real-time power generation control algorithm (IRPGC). Finally, a real-time integrated scheduling and control framework for microgrids is established. The research aims to achieve superior control performance while addressing the divergence issues in microgrid systems and the shortcomings in economic dispatch and frequency control in microgrid applications.

The two main innovations of the study are as follows. First, the IRPGC algorithm is designed to address the real-time generation scheduling and control challenges posed by the large-scale integration of new energy and users into microgrids. Second, a real-time integrated scheduling and control framework is established for microgrids to guide for the intelligent construction of integrated energy systems. The structure of the research is divided into four main sections. Section 2 presents a review of relevant research findings. Section 3 presents the design of the DNN-ADP algorithm and the IRPGC algorithm, along with the construction of the real-time integrated scheduling and control framework for microgrids. Section 4 focuses on validating the effectiveness and feasibility of the proposed method. Section 5 summarizes the research.

2 Related works

With the continuous growth in energy demand, traditional fossil fuels are increasingly facing a crisis of depletion, leading to serious ecological and environmental pollution issues. Therefore, the development of renewable energy and sustainable practices has become a research focus. Real-time power generation control has become a key means to achieve these goals. Numerous scholars conducted in-depth analyses and discussions on this subject. Zeinal-Kheiri *et al.* proposed a real-time adaptive microgrid energy scheduling method based on Lyapunov optimization, combined with a stochastic day-ahead French real-time energy management system. The research results demonstrated a reduction in real-time operational costs for the microgrid, confirming the effectiveness of the method in improving performance [8]. Wang *et al.* designed a model predictive control algorithm to address optimal energy management issues, utilizing two different power sources to achieve fuel economy and emission reduction goals. Experimental results indicated that the algorithm could ensure optimal results, with an approximately 5.2% improvement in fuel economy compared with rule-based control strategies [9]. Due to a lack of precise assessment and configuration studies on the control capabilities of variable-speed constant-frequency pumped storage hydropower, Zhang *et al.* focused on a cascade hydropower-photovoltaic-variable-speed constant-frequency pumped storage hydropower system. A rule-based method for determining adjustment capacity was proposed. The results indicate that this method is effective in suppressing rapid fluctuations in photovoltaic systems in real time [10]. Fang *et al.* identified that frequent adjustments in real-time power output from concentrated solar power could impact the durability and profitability of factories. Therefore, an optimal bidding strategy for energy and frequency regulation was developed. It was applied to the coordinated operation of concentrated solar and wind farms in the market recently [11].

DNN has broad application prospects in the field of the power grid, which can be used to monitor the operation status of the power grid in real time, predict future electricity demand, and forecast the generation of renewable energy. By employing real-time power generation regulation, DNNs enhance the operational efficiency and reliability of the power grid. Zhao and Hanglin explored compression techniques without compromising DNN performance. A DNN optimization compression algorithm based on a hybrid mechanism was proposed. Experimental results on the mini-ImageNet dataset indicated that even with a 6.3% reduction in compression accuracy, the algorithm achieved a remarkable 98.5% reduction in the capacity of the compressed AlexNet [12]. Chen *et al.* introduced an effective method for detecting internal voids in wood to ensure structural safety. The DNN was used for the analysis. The experimental results demonstrated high accuracy and generality in identifying the severity of voids [13]. In response to the demand for high-precision indoor positioning in location-based services and emerging Internet-of-things applications, Chen *et al.* designed a scene analysis positioning solution based on a multidetector DNN architecture. The results showed that this method effectively addressed the complex linear relationship between fingerprints and spatial locations [14]. To tackle challenges in resource allocation for energy-saving in multicell carrier nonorthogonal multiple access under interference and other factors, Adam *et al.* proposed a real-time power allocation using a dual-channel enhanced DNN. Simulation results indicated the suitability of this method for real-time applications [15].

To sum up, it is obvious that the current research mainly focuses on the control of power systems and the application of the DNN algorithms. Traditional intelligent control strategies face challenges in addressing economic dispatch and frequency control in microgrids. To provide effective control methods for large-scale microgrid systems that handle numerous energy sources, the study designs

the DNN-ADP algorithm and the IRPGC algorithm, establishing a real-time integrated scheduling and control framework for microgrids.

3 Real-time integration framework for microgrid based on DNN

In the context of dual carbon, the installed capacity and power generation of new energy in China have grown rapidly. At the same time, the high proportion of renewable energy and emerging loads connected to the power grid will cause complex control, source load fluctuations, and mechanism ambiguity, which poses a huge challenge to the stable and safe operation of the power grid. Therefore, the research first introduces the ADP algorithm to construct the DNN-ADP algorithm based on the DNN algorithm. Then, it is optimized by introducing rejection operations to construct the IRPGC algorithm. Finally, a real-time integrated scheduling and control framework for microgrids is established.

3.1 Design of DNN-ADP

Microgrid is a complex distributed system with various types of power sources and loads. The corresponding power supply has characteristics such as indirectness and uncertainty, with significant frequency fluctuations [16,17]. Traditional control strategies struggle to adapt to the rapid changes in microgrids and cannot achieve the economic and real-time operation of microgrids, resulting in poor performance in economic dispatch and frequency control in microgrids. Due to the limitation of the DNN algorithm on the real-time scheduling accuracy of microgrids, the DNN-ADP algorithm is designed based on the DNN algorithm combined with the ADP algorithm. The algorithm includes four multioutput DNNs: execution network, model prediction network, evaluation network 1, and evaluation network 2. The ADP algorithm can effectively handle optimization problems for discrete and continuous systems and stop when obtaining the optimal control law or reaching the set maximum number of iterations. The specific process of the DNN-ADP algorithm is as follows. First, the ADP algorithm iteratively approximates the true solution of dynamic programming, thereby approximating the optimal control solution of nonlinear systems in microgrids. The ADP algorithm has four basic structures: heuristic dynamic programming (HDP), performing dependency-heuristic dynamic programming (PDHDP), bi-heuristic dynamic programming (Bi-HDP), and performing dependent dual heuristic dynamic programming (PDDHDP) [18]. The schematic diagram of the four basic structures of the ADP algorithm is shown in Figure 1.

The basic structural diagrams of HDP, PDHDP, Bi-HDP, and PDDHDP are shown in Figure 1(a)–(d). For the $k+1$ segment, $x(k)$ is the starting state, which is jointly generated by the $u(k)$ controlled by the previous k segment. $U(x(k))$ is the feedback control variable. The input variables are mapped from the state variables to the control variables through the execution network. Then, the model network constructs a model for the nonlinear system. Finally, the performance indicator function of the neural network can be output by evaluating the network. Assuming the weight of the evaluation network is ω, differential processing can be performed. The corresponding continuous partial derivatives can be obtained through and the output

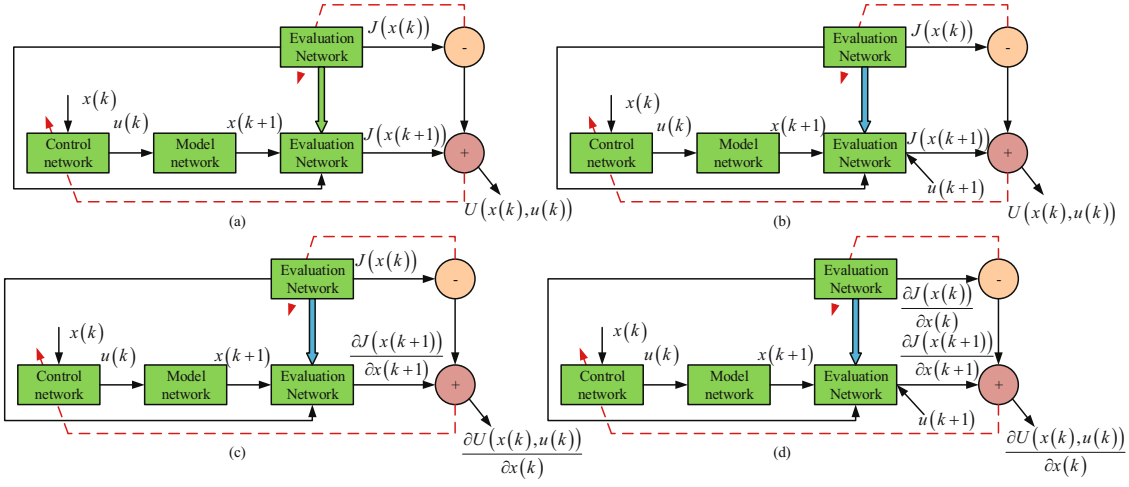

Figure 1: Schematic diagram of four basic structures of the ADP algorithm. (a) HDP structure. (b) PDHDP structure. (c) Bi-HDP structure. (d) PDDHDP structure.

of different network structures. The next state is calculated through $x(k+1) = d[x(k), u(k)]$, and d is the control process calculation function. In HDP, there are three components: the execution network, model network, and evaluation network, corresponding to the input and output of state variables and performance indicator functions. In PDHDP, a part of the execution network serves as the input to the evaluation network. The remaining functions are similar to the ADP algorithm. Bi-HDP includes the model network, evaluation network, and control network. Unlike HDP, it approximates the objective function, which makes the training of the evaluation network more complex. PDDHDP is similar to Bi HDP in maintaining consistency, but has higher control accuracy because it takes control variables and system states as inputs. In the ADP algorithm, it starts with assuming an initial point as the estimated cost. After each optimization iteration, adjustments are made to the control law and cost function correction values. After multiple iterations, the policy improvement procedure and value determination operation generate corresponding suboptimal control law c_l and cost function J_l. If they converge to optimal control and optimization functions, the process can be stopped. In the policy improvement procedure, a cost function $J(*, c_l)$ corresponding to a certain state c_l is given. The optimized control law c_{l+1} can be obtained, as shown in Eq. (1).

$$c_{l+1}(x_k) = \arg\min_{u_k} \{U(x_k, u_k) + J(x_{k+1}, c_l)\}. \tag{1}$$

In Eq. (1), x_k represents state variables, u_k belongs to the controlled variables, k denotes a change in time during dynamic variations, U is the control set, and l represents the lth iteration in the optimization process. In the value determination operation, the expression for transforming the cost function for any control law is given by Eq. (2).

$$J_{l+1}(x_k, c) = U(x_k, u_k) + J(x_{k+1}, c_l). \tag{2}$$

When dealing with the control problem of microgrid power generation, the control area is simplified and treated as having only one generator. This results in the state space equation for region i, as shown in Eq. (3).

$$\begin{cases} \dot{x} = A_i x_i + B_i u_i + \sum_{j=1, j\neq i}^{N} A_{ij} x_j + G_i \Delta p_{L_i}, \\ i = 1, \ 2, \ \ldots, \ N \\ x_i = [\Delta g_i, \ \Delta p_{m_i}, \ \Delta p_{v_i}, \ \Delta p_{te}^{ij}]^T \\ u_i = \Delta p_{c_i} \\ A_{ij} = \begin{bmatrix} 0 & 0 & 0 & 0 \\ 0 & 0 & 0 & 0 \\ 0 & 0 & 0 & 0 \\ -T_{ij} & 0 & 0 & 0 \end{bmatrix}. \end{cases} \tag{3}$$

In Eq. (3), A_i, B_i, A_{ij}, and G_i are state matrices; Δp_{L_i}, Δg_i, Δp_{m_i}, Δp_{v_i}, and Δp_{c_i} represent the load, frequency deviation, generator mechanical power deviation, turbine governor position deviation, and power at the load reference point for region i, respectively; Δp_{c_i} represents the exchange power between regions i and j; and T is the time constant. The dynamic model expressions for Δg_i, Δp_{m_i}, Δp_{v_i}, and Δp_{c_i} are given in Eq. (4).

$$\begin{cases} \Delta \dot{g}_i = -\frac{D_i}{M_i} \Delta g_i + \frac{1}{M_i} \Delta p_{m_i} - \frac{1}{M_i} \Delta p_{te}^{ij} - \frac{1}{M_i} \Delta p_{L_i} \\ \Delta \dot{p}_{m_i} = -\frac{1}{T_{eh_i}} \Delta p_{m_i} + \frac{1}{T_{ch_i}} \Delta p_{v_i} \\ \Delta \dot{p}_{v_i} = -\frac{1}{R_i T_{f_i}} \Delta g_i - \frac{1}{T_{f_i}} \Delta p_{v_i} + \frac{1}{T_{f_i}} \Delta p_{e_i} \\ \Delta \dot{p}_{te}^{ij} = \sum_{j=1, j\neq i}^{N} T_{ij} (\Delta g_i - \Delta g_j). \end{cases} \tag{4}$$

In Eq. (4), D_i, M_i, and T_{f_i} are the damping coefficient, rotational inertia, and time constant of the generator, respectively; R_i and T_{ch_i} are the speed damping coefficient and turbine time constant for region i, respectively; and T_{ij} represents the synchronization time factor. The convergence analysis of the aforementioned dynamic model is conducted through previous research methods [19,20]. In the reinforcement learning part of the DNN-ADP algorithm, the maximum cumulative reward is achieved through the interaction between intelligent agents and the environment. Initially, the policy $\pi(a|s)$ is defined, representing the relationship between state S_t and action A_t. The probability P of the outputting action a for any input s is given in Eq. (5):

$$\pi(a|s) = P\{A_t = a|S_t = s\}. \tag{5}$$

The input s in Eq. (5) belongs to the state set S. The quality judgment of the state–action pair formed by s_t and a_t at time t is determined through the accumulated rewards. Therefore, the discount factor γ is used to calculate the cumulative reward value R_t, as shown in Eq. (6):

$$R_t = \sum_{k=0}^{\infty} \gamma^k r_{t+k}. \tag{6}$$

In Eq. (6), r_t and r_{t+k} represent immediate rewards and subsequent rewards at step k, respectively. The state–action value function $Q^{\pi}(s, a)$ is shown in Eq. (7) [21].

$$Q^{\pi}(s, a) = E_{\pi}[R_t|S_t = s, \quad A_t = a]. \tag{7}$$

Based on Eq. (7), the optimal policy, represented by the maximized $Q^*(s, a)$, can be learned. For ease of subsequent solution, the Bellman equation is introduced for iterative computation, as shown in Eq. (8) [22,23].

$$Q^*(s, a) = R_s^a + \gamma \sum_{s' \in S} P_{ss'}^a \max_{a'} Q^*(s', a'). \quad (8)$$

In Eq. (8), s and a are the current state and actions, respectively; s' and a' are the next-step state and action; and $P_{ss'}^a$ represents the probability of transitioning from state s to state s' using action a. The most representative algorithm in reinforcement learning is the Q-learning algorithm, as shown in Eq. (9) [24,25].

$$Q_{t+1}(s_t, a_t) = Q_t(s_t, a_t) + \alpha[r_{t+1} + \gamma \max_{a'} Q(s_{t+1}, a') - Q(s_t, a_t)]. \quad (9)$$

In Eq. (9), α represents the learning rate. The flowchart of the Q-learning algorithm is illustrated in Figure 2.

In Figure 2, to ensure the convergence of the current algorithm by calculating the tolerance between the estimated value and the old value, the study introduces the ε-graddy algorithm, which can effectively solve the contradiction between exploration and utilization in reinforcement learning and improve the convergence efficiency of the algorithm. Finally, in the DNN section, the perceptual and decision-making capabilities of deep learning are combined with reinforcement learning to achieve better results. Combining all the aforementioned factors, the DNN-ADP algorithm is obtained. Its corresponding structural diagram is shown in Figure 3.

In Figure 3, the DNN-ADP algorithm is derived from DNN by combining the ADP algorithm. This helps improve the optimization and control performance of microgrids and accelerates the convergence and real-time updating of learning results.

3.2 Construction of the IRPGC algorithm and real-time integrated scheduling and control framework for microgrids

To effectively address the stability, flexibility, and reliability in microgrid generation scheduling control, as well as uncertainties and disturbances from the external environment, the study introduces the rejection operation. Based on the DNN-ADP algorithm, the IRPGC algorithm is proposed, which can output multiple power generation commands at once for microgrid control. This addresses the shortcomings in economic scheduling and frequency control. Traditional reinforcement learning methods require training or reinforcing each action, which consumes a long time. Although the accuracy of the trained IRPGC algorithm may not be entirely correct, even if some actions are trained by the algorithm, it can provide more accurate output, which requires more computer memory. The IRPGC algorithm based on DNN utilizes two or more stacked-constrained Boltzmann machines. In the training phase, unsupervised layerwise greedy training is performed, followed by supervised learning to train the network after offline training

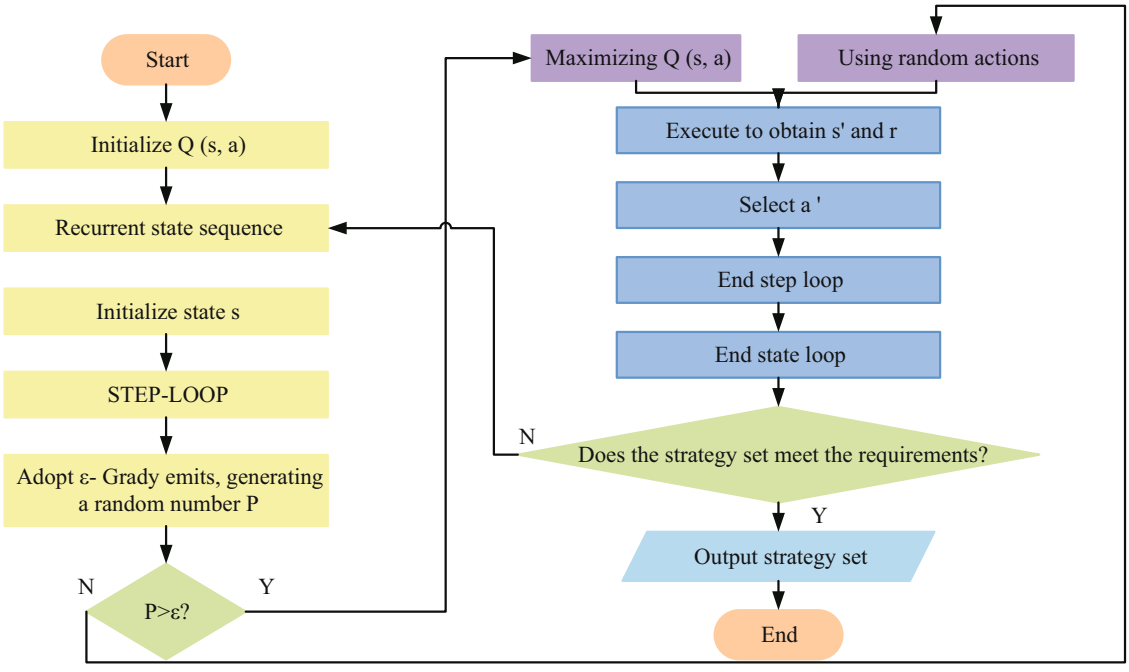

Figure 2: Q-learning algorithm flowchart.

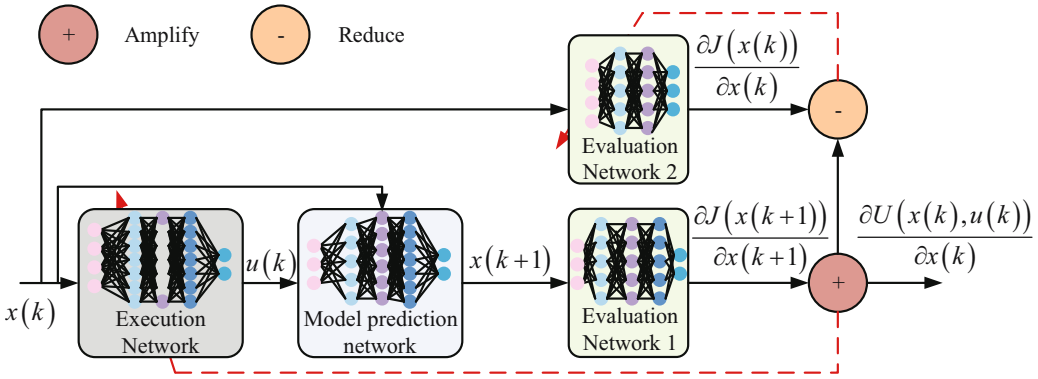

Figure 3: Schematic diagram of the DNN-ADP algorithm structure.

completion. The IRPGC algorithm does not require the collaborative coordination of other optimization algorithms and can optimize computational efficiency and memory space. The schematic diagram illustrating the specific convergence acceleration principle of the IRPGC algorithm is shown in Figure 4.

In Figure 4, the predictive network can perform advance predictions on the microgrid system to assess the effects after a specific action is executed. This ultimately accelerates the convergence process. In the non-recognition (NR) operation part of the IRPGC algorithm, to address the low reliability of action commands when the probability values at the output layer corresponding to evaluation network 1 are low, the IRPGC algorithm employs the DNN-ADP algorithm to obtain new power generation commands. For ease of subsequent control, the NR operation relies solely on a simple rejection threshold, as calculated in Eq. (10).

$$\Delta P^* = \begin{cases} \Delta P, & T_{\mathrm{DP}} > T \\ y_{\mathrm{PID}}, & T_{\mathrm{DP}} \le T. \end{cases} \tag{10}$$

In Eq. (10), ΔP^* represents the power generation command corrected through the NR operation, ΔP represents the power generation command output by the IRPGC algorithm, and T and T_{DP} are the rejection threshold and the output layer probability value of the DNN-ADP algorithm, respectively. These are proportional-integral-derivative (PID) control algorithm outputs. The research utilizes the DNN to output the results of evaluation network 1 when it knows it is more important. In cases where it is unaware of its importance, the rejection operation is chosen, and y_{PID} is output. The power generation command for intelligent power generation control in the microgrid is output through the controller, where the system state of the microgrid environment is represented by Δg, the action values are set as an $n*m$ matrix, and n and m correspond to the quantity of units and the quantity of instructions generated by each unit, respectively. The action matrix A is given by Eq. (11).

$$A = \begin{bmatrix} A_1^1 & A_2^1 & \cdots & A_n^1 \\ A_1^2 & A_2^2 & \cdots & A_n^2 \\ \vdots & \vdots & \ddots & \vdots \\ A_1^m & A_2^m & \cdots & A_n^m \end{bmatrix}. \tag{11}$$

According to the principle of a single hidden layer feedforward neural network used in the algorithm, it can be known that for any number of different samples, there is no limit to the interval and the function is infinitely differentiable. In the case of uncertain assignment, the corresponding action matrix is reversible. In this way,

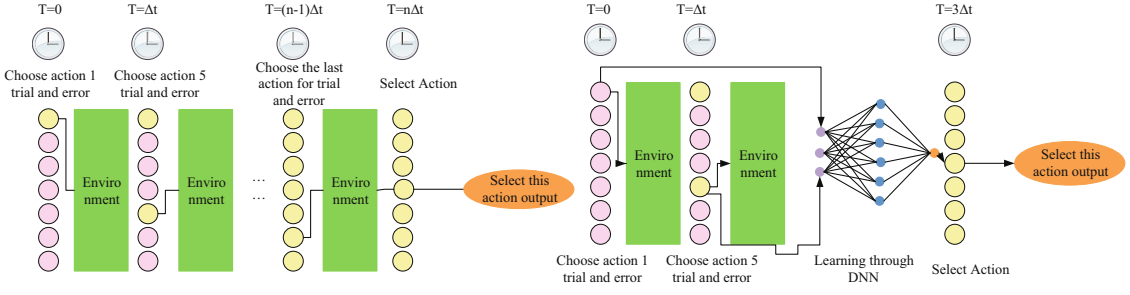

Figure 4: Schematic diagram of the IRPGC algorithm accelerating convergence principle.

the execution process of the IRPGC algorithm is obtained, as shown in Figure 5.

In Figure 5, after the four DNNs undergo computation in the algorithm, a comparison is made between the output layer probability values of evaluation network 1. Finally, a judgment is made, and action values are output. Based on the aforementioned content, to obtain better control performance indicators and the stability of microgrid systems, this study is similar to the stability of numerical analysis, that is, the sensitivity of algorithms to rounding errors, and investigates the regulation from economic dispatch and frequency control. In addition, to address the shortcomings of traditional control strategies in realizing regulation in these two aspects of microgrid control, the study constructs a combined scheduling and control framework for the microgrid. This framework coordinates economic scheduling with automatic power generation control and droop control. In the droop control section, the transformer at the interface of distributed power sources is controlled to exhibit generator active power and frequency characteristics, as calculated in Eq. (12) [26,27].

$$f = f_0 + mp_q(p_{\mathrm{ref}_q} - p_q). \tag{12}$$

In Eq. (12), f and f_0 represent the frequency and rated frequency of the microgrid, respectively; q denotes the qth distributed power source; and mp_q, P_{ref_q}, and P_q correspond to the droop coefficient, active power reference value, and output value associated with the qth distributed power source, respectively. Since the system frequency in this part is determined by the system load, the study investigates the automatic generation control within the framework to reduce frequency deviation. In the intelligent generation control section, it is necessary to satisfy the balance constraint $\sum_{n=1}^{n} P_q = P_d$. When the total load changes to ΔP, the corresponding power allocation expression can be obtained, as shown in Eq. (13).

$$\Delta P_q = \frac{mP_{\mathrm{MG}}}{mP_Q}\Delta P. \tag{13}$$

In Eq. (13), mP_{MG} represents the equivalent value of the droop coefficient in the microgrid system. Finally, the value of P_{ref_q} is assigned to $P^*_{\mathrm{ref}_q}$, enabling coordination between economic dispatch and intelligent generation control at the same time scale. In the economic dispatch section, the calculated output of the generation controller

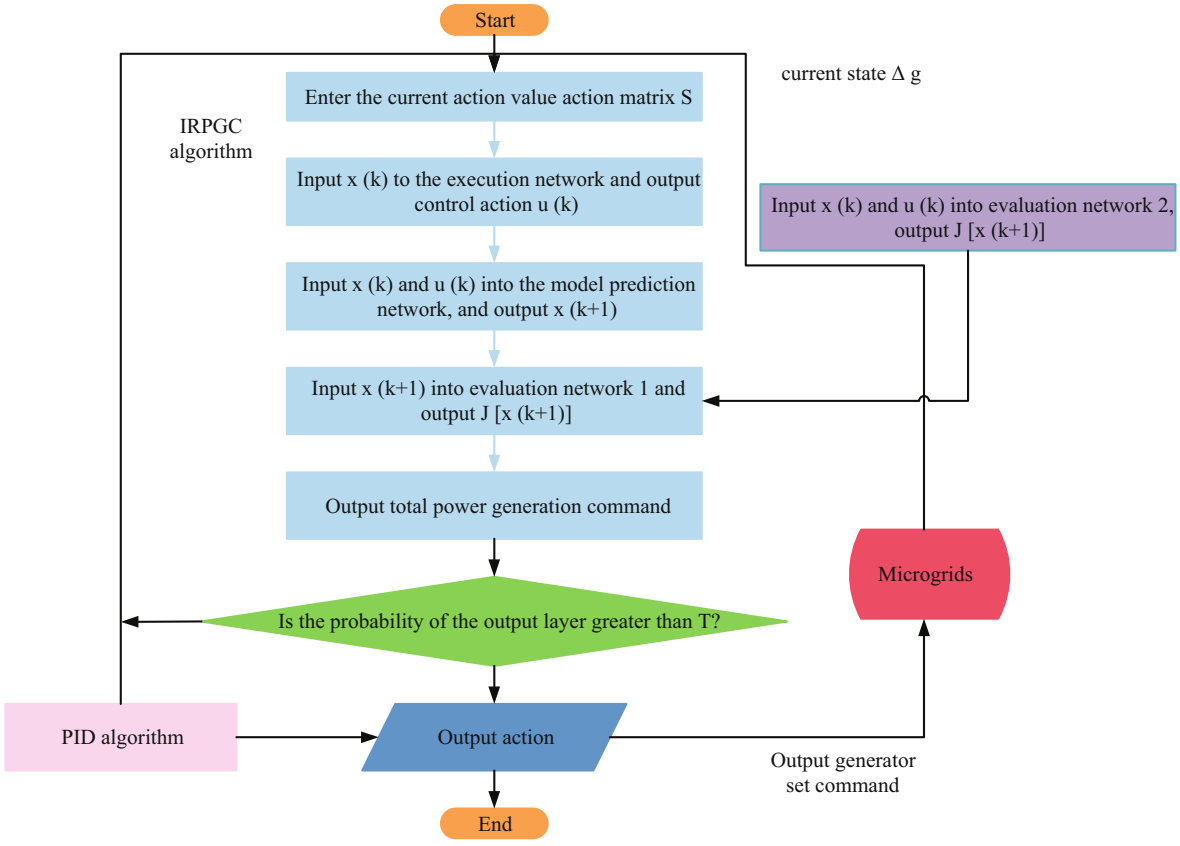

Figure 5: IRPGC algorithm execution process.

combining droop control, intelligent generation control, and economic dispatch is given by Eq. (14).

$$P_{\mathrm{ED}} + \Delta P_q + P_{\mathrm{ref}_q}. \tag{14}$$

In Eq. (14), P_{ED} represents the dispatchable active power corresponding to q. To minimize the economic cost of generation control, the expression for generation cost is derived, as shown in Eq. (15) [28]:

$$\begin{cases} \min C_{ct} = \sum_{q=1}^{n} (a_q P_{\mathrm{ED}_q}^2 + b_q P_{\mathrm{ED}_q} + c_q) \\ s.t. \begin{cases} \sum_{q=1}^{n} P_{\mathrm{ED}_q} = P_d \\ P_q^{\min} \le P_{\mathrm{ED}_q} \le P_q^{\max}. \end{cases} \end{cases} \tag{15}$$

In Eq. (15), a_q, b_q, and c_q are the cost coefficients corresponding to q; P_d represents the predicted energy demand of the microgrid; and $P_q^{\min}$ and $P_q^{\max}$ are the minimum and maximum active power, respectively, corresponding to q. Combining the aforementioned content, a real-time integrated scheduling and control framework for the microgrid can be constructed, as illustrated in Figure 6.

In Figure 6, the IRPGC algorithm takes into account both long-time scale economic dispatch information and real-time control frequency deviation information, replacing traditional dispatch control frameworks.

4 Results analysis of real-time economic dispatch and frequency control in microgrid based on IRPGC algorithm

To assess the effectiveness and feasibility of real-time economic dispatch and frequency control in microgrids based on the IRPGC algorithm, comparative experiments are conducted on the performance of the algorithm. Subsequently, simulations are carried out in practical applications.

4.1 Performance analysis of real-time economic dispatch and frequency control in microgrid based on IRPGC algorithm

To validate the performance of the proposed IRPGC algorithm, the simulation environment is set up using the Windows 10 operating system on a computer with 16GB of RAM. The experiments are conducted using MATLAB software. In addition, to demonstrate the feasibility and superiority of the proposed real-time integrated scheduling and control framework for microgrids, the study selects

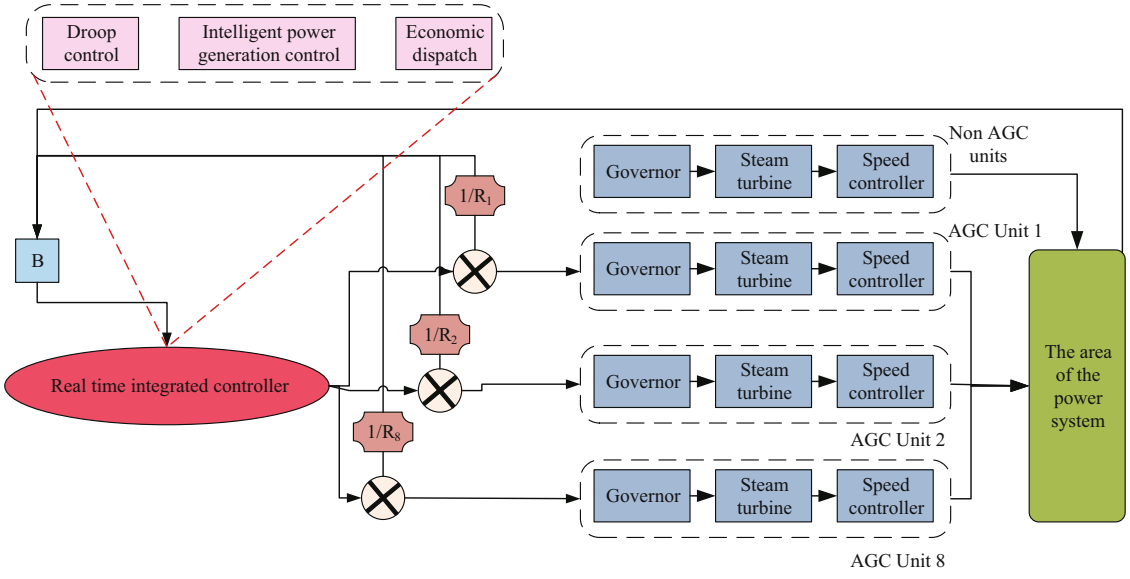

Figure 6: Real-time integrated scheduling and control framework for microgrids.

Table 1: Economic dispatch parameter settings corresponding to microgrid data

Parameter	Alternator							
	1	2	3	4	5	6	7	8
a_q ($/MW^2)	0.677	0.452	0.565	0.565	0.4521	0.565	0.565	0.339
b_q ($/MW)	370	250	310	310	250	310	310	191
c_q ($)	11,260	7,610	9,490	9,490	7,610	9,490	9,490	5,630
$P_q^{\min}$ (MW)	20	110	160	30	20	60	20	20
$P_q^{\max}$ (MW)	80	220	745	150	70	242	62	90

microgrid data from Hainan power grid for experimentation. This microgrid serves 200 million households in an area of 3.4×10^{11} m^2. The microgrid includes three energy sources and power loads: wind power generation, photovoltaic power generation, electric vehicles, household loads, and eight automatic generators. The frequency reference coefficient is set to 70. The economic dispatch and intelligent power generation control periods are set at 300 and 5 s, respectively. The time constants for the governor, generator, and turbine are set at 0.08, 0.03, and 10, respectively. Finally, the economic dispatch parameters for the microgrid data are presented in Table 1.

To scientifically evaluate the performance of the proposed algorithm and the real-time integrated framework for microgrids, the proposed method is with mainstream frameworks. The intelligent power generation control algorithms include PID, fractional order PID (FO-PID), active disturbance rejection controller (ADRC), sliding mode control (SMC), and fuzzy logic control (FLC). Correspondingly, the economic dispatch optimization algorithms include simulated annealing, particle swarm optimization, genetic algorithm, multivariate optimization algorithm (MOA), and grey wolf algorithm (GWA). MOA is a swarm intelligence optimization algorithm with clear individual division of labor and collaborative cooperation, which has the diversified characteristics of different divisions of labor. GWA is a traditional GWA optimized by improving the convergence factor strategy and dynamic weight strategy. To assess the robustness of the IRPGC algorithm under complex conditions, the study introduces 10% random disturbance power and load, adds to wind and photovoltaic power, considers five different charging behaviors for electric vehicles, and overlays them on the electric vehicle power curve. Finally, typical household loads from real-life scenarios are introduced.

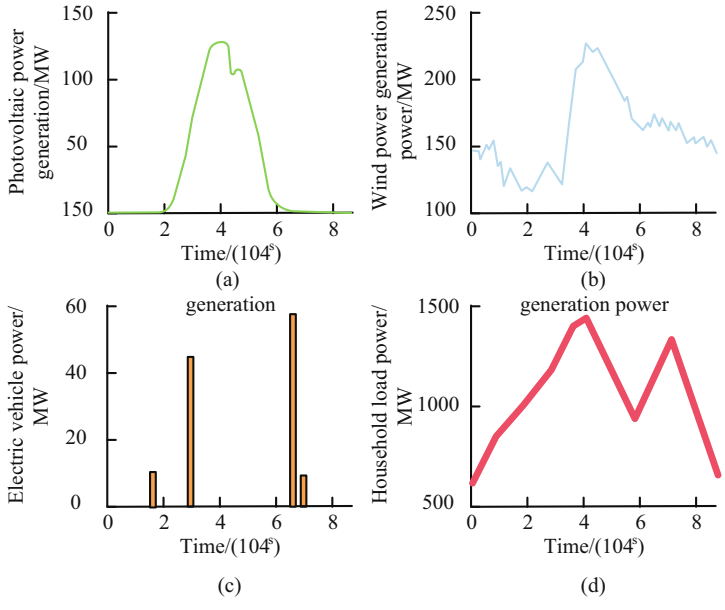

Figure 7: Different types of power variation curves in microgrid data. (a) Photovoltaic power. (b) Wind power. (c) Electric vehicle power. (d) Household load power.

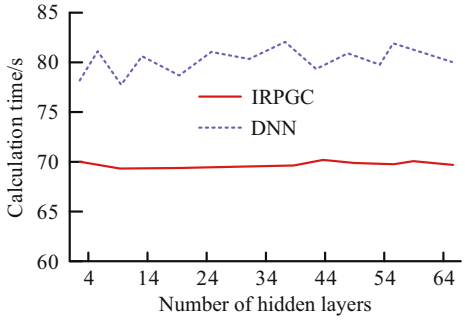

Figure 8: The variation curve of the number of hidden layers and computation time for different neural network structures.

Figure 7(a)–(d) corresponds to the power variation curves of photovoltaic power generation, wind power generation, electric vehicle power, and household load in the Hainan microgrid data, respectively. From Figure 7, the four power variation curves exhibited overall periodic changes. Photovoltaic power generation, wind power generation, and household load power reached their peaks around 410^4 s, while the power of electric vehicles reached its peak around 710^4 s. When training the DNN of the IRPCC algorithm, the visible layer input and output units are set to 3 and 8, respectively, and the number of hidden layer units is set to [24, 60, 64, 8]. The maximum number of iterations is set to 1,000, and the learning rate is set to 0.1.

First, it is necessary to verify the improvement effect of the number of hidden layers in different neural network structures on system computation time, as shown in Figure 8. From Figure 8, as the number of hidden layers increased, both DNN and IRPGC algorithms fluctuated within a certain calculation time range, and the variation curve of the IRPGC algorithm was smoother and the fluctuation range was smaller. The average computation time for different neural network structures is calculated for the analysis. The average computation time for DNN was 81.963 s, while the average computation time for the IRPGC algorithm was 67.245 s, with a reduction of 14.718 s. In terms of computation time, the IRPGC algorithm increased by 17.96%, indicating that the research algorithm greatly improves computation time and efficiency.

The average error results during the training phase of the IRPGC algorithm based on Hainan microgrid data are shown in Figure 9. From Figure 9, after 5,000 iterations, the average error of the IRPGC algorithm remained within 10^{-5}. In addition, by conducting the stability analysis based on mathematical foundations, Eq. (16) is obtained.

$$\begin{cases} \lim\limits_{i\to\infty} u_i(x_k) = u^*(x_k) \\ \lim\limits_{i\to\infty} J_i(x_k) = J^*(x_k). \end{cases} \tag{16}$$

Eq. (16) indicates that the system based on the IRPGC algorithm framework proposed in the study is stable. To better evaluate the control performance of different algorithms, common metrics such as mean error integral (MEI), absolute error integral (AEI), and time-weighted absolute error integral (TWAEI) are chosen for evaluation. TWAEI is mainly an integral expression of a function that represents the deviation between the expected output and the actual output of the system, which is used to measure the performance of the control system. The AEI index is used to evaluate the role of the system during the transition process.

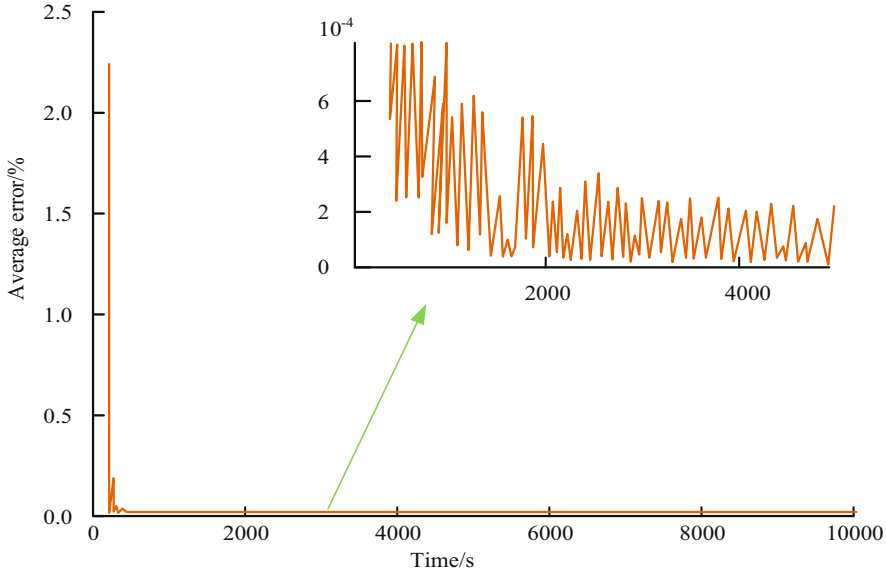

Figure 9: The average error results during the training phase of the IRPGC algorithm based on Hainan microgrid data.

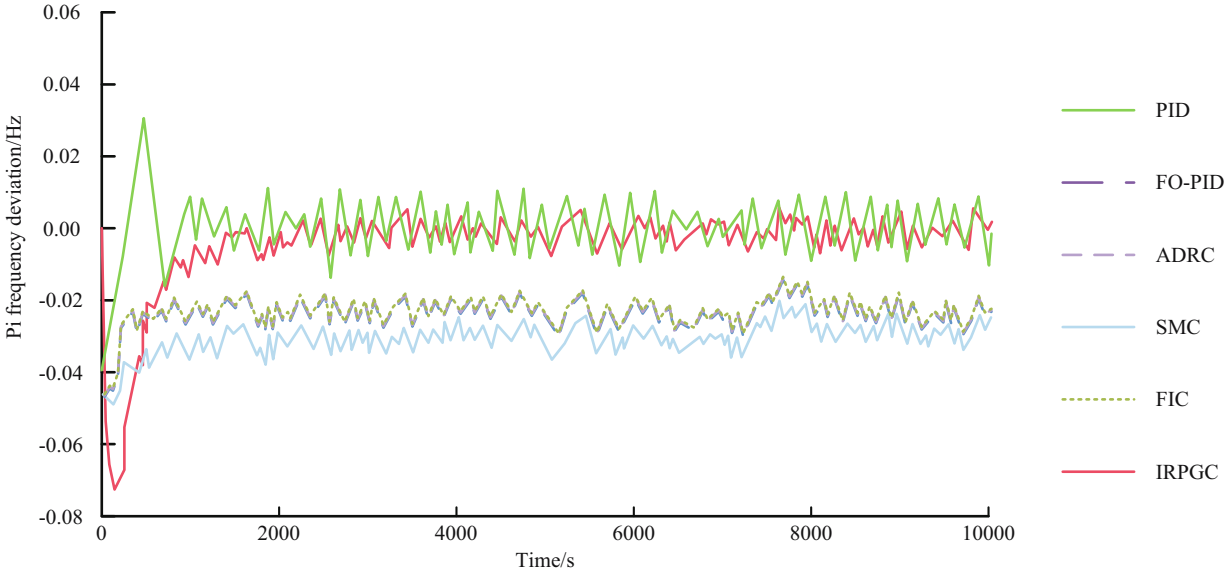

Figure 10: Comparison of frequency deviation results of different algorithms based on Hainan microgrid data.

The comparison of frequency deviation results for different algorithms based on Hainan microgrid data is shown in Figure 10. According to Figure 10, the frequency deviation ranges corresponding to PID, FO-PID, ADRC, SMC, FLC, and IRPGC were −0.04 to 0.037 Hz, −0.046 to 0.019 Hz, −0.047 to 0.0187 Hz, −0.049 to −0.02 Hz, −0.043 to −0.0191 Hz, and −0.073 to 0.013 Hz, respectively. The above results may be due to the fact that the research algorithm can effectively replace traditional microgrid power generation scheduling control frameworks and be applied in real-time microgrid power generation scheduling control frameworks. Moreover, from the long-term overall change curve, the frequency deviation values were mostly negative, indicating that the frequency deviation is opposite to the power generation instructions obtained through economic dispatch and intelligent power generation controllers.

Figure 11(a) and (b) presents the results of different frequency deviation evaluation indicators and rejection operation outcomes based on the IRPGC algorithm, respectively. In Figure 11(a), the MEI indicators corresponding to PID, FO-PID, ADRC, SMC, FLC, and IRPGC were 62.21, 254.24, 243.96, 309.61, 244.89, and 51.45, while the AEI indicators were 1.73, 6.11, 6.09, 9.72, 6.24, and 0.54, respectively. The TWAEI indicators corresponded to 2.15×10^5, 11.96×10^5, 11.95×10^5, 14.85×10^5, 11.99×10^5, and 1.58×10^5. In the aforementioned error integration results, all indicators of the research algorithm have the lowest values, with the AMI indicator reaching 0.54. This means that the proposed system has minimal errors in mathematical analysis, while the MEI indicator indicates that the research method has a good transient response and appropriate damping. This is because the intelligent power generation controller and

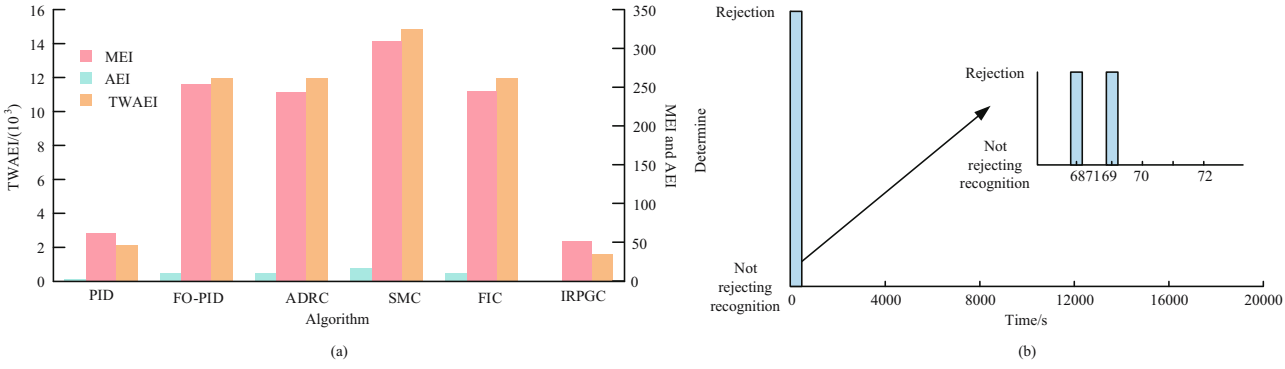

Figure 11: Evaluation index results and rejection operation results of different frequency deviations based on the IRPGC algorithm. (a) Results of evalutation indicators for different frequency deviations based on the IRPGC algorithm. (b) Reject operation result.

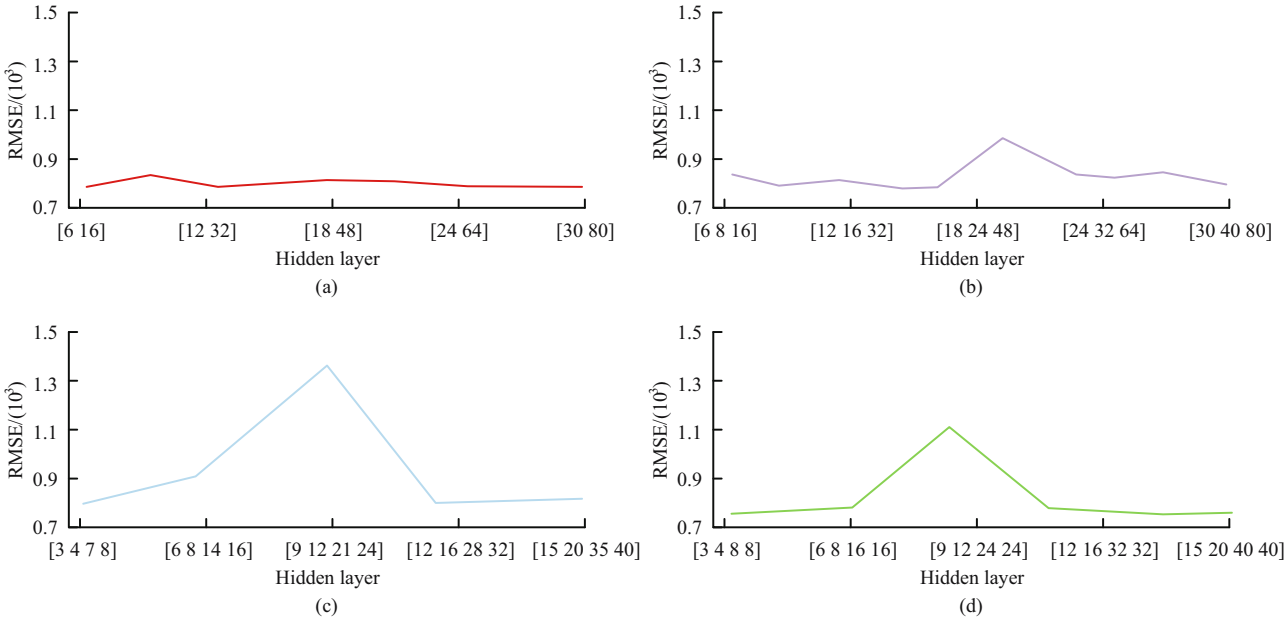

Figure 12: RMSE results of hidden layer for different applications based on the IRPGC algorithm. (a) Stage 1. (b) Stage 2. (c) Stage 3. (d) Stage 4.

economic dispatch in the system framework will optimize their respective optimization objectives separately, providing a precise adjustment command with a unified time scale. Therefore, the performance of all aspects can be significantly optimized. As shown in Figure 11(b), the rejection operation using the IRPGC algorithm is simulated 69 s earlier. Afterward, the probability value of the output layer corresponding to network 1 in the algorithm always exceeds the set threshold. Overall, the IRPGC algorithm effectively fits random disturbances in the power flow, resulting in a significant improvement in control performance. In conclusion, the proposed IRPGC algorithm exhibits excellent control performance and stability, making it suitable for integrated scheduling and control in microgrids.

4.2 Application analysis of real-time economic dispatch and frequency control in microgrid based on IRPGC algorithm

The aforementioned results confirmed the superior control performance of the IRPGC algorithm. To further explore the practical application effects of the algorithm in real-time generation scheduling and control frameworks in microgrids, experiments were conducted using data from the Sanya microgrid. The DNN of the IRPGC algorithm and the corresponding hidden layer ranges were [3, 10] and [8, 400], respectively, taking root-mean-square error (RMSE) as an indicator.

Figure 12(a)–(d) shows the RMSE results for stages 1–4 of the hidden layers based on the IRPGC algorithm. From Figure 12, in the application of real-time generation scheduling and control, the optimal rejection threshold range based on the IRPGC algorithm was [0.94, 0.97]. These results indicate that the IRPGC algorithm has good feasibility and applicability in practical applications.

5 Conclusion

In recent years, microgrids have been widely applied. However, ensuring the frequency stability of microgrids and maintaining a balance between economic and environmental benefits has been a research focus. To address these issues, the study initially integrated the ADP algorithm into the DNN, resulting in the DNN-ADP algorithm. Subsequently, the rejection operation was introduced to obtain the IRPGC algorithm. Finally, a real-time integrated scheduling and control framework for microgrids was established. From experimental results, after 5,000 iterations during the training phase, the IRPGC algorithm exhibited an average error within the range of 10^{-5}. The frequency deviation ranges corresponding to PID, FO-PID, ADRC, SMC, FLC, and IRPGC were −0.04 to 0.037 Hz, −0.046 to 0.019 Hz, −0.047 to 0.0187 Hz, −0.049 to −0.02 Hz, −0.043 to −0.0191 Hz, and

−0.073 to 0.013 Hz, respectively. In terms of the three frequency deviation evaluation indicators, MEI indicators for PID, FO-PID, ADRC, SMC, FLC, and IRPGC were 62.21, 254.24, 243.96, 309.61, 244.89, and 51.45, while AEI indicators were 1.73, 6.11, 6.09, 9.72, 6.24, and 0.54, respectively. The TWAEI indicators corresponded to 2.1510^5, 11.9610^5, 11.9510^5, 14.8510^5, 11.9910^5, and 1.5810^5. In the practical application of real-time generation scheduling and control in the microgrid, the optimal rejection threshold range based on the IRPGC algorithm was found to be [0.94, 0.97]. In conclusion, the proposed IRPGC algorithm demonstrated good economic control performance and frequency control performance, effectively addressing complex control issues in microgrids. However, there are still limitations in the research. There is a significant computational load in practical applications. Therefore, in future research, this method can be further lightweight to improve computational efficiency.

Funding information: The research was supported by Natural Science Research Project of Shangluo University (No. 24KYZX03).

Author contributions: All the contributions related to the paper are attributed to Jun Liu. The author confirms the sole responsibility for the conception of the study, presented results and manuscript preparation.

Conflict of interest: Author states no conflict of interest.

Data availability statement: The datasets generated during and/or analysed during the current study are available from the corresponding author on reasonable request.

References

[1] Kumar S, Das P, Kumar K. Adaptive mesh based efficient approximations for Darcy scale precipitation–dissolution models in porous media. Int J Numer Methods Fluids. 2024;96(8):1415–44.

[2] Saini S, Das P, Kumar S. Computational cost reduction for coupled system of multiple scale reaction diffusion problems with mixed type boundary conditions having boundary layers. RACSAM. 2023;117(2):66.

[3] Shiromani R, Shanthi V, Das P. A higher order hybrid-numerical approximation for a class of singularly perturbed two-dimensional convection-diffusion elliptic problem with non-smooth convection and source terms. Comput Math Appl. 2023;142:9–30.

[4] Yao A, Sheng W. Interaction of elementary waves on a boundary for a hyperbolic system of conservation laws. Math Methods Appl Sci. 2008;31(11):1369–81.

[5] Santra S, Mohapatra J, Das P, Choudhuri D. Higher order approximations for fractional order integro-parabolic partial differential equations on an adaptive mesh with error analysis. Comput Math Appl. 2023;150:87–101.

[6] Kumar K, Podila PC, Das P, Ramos H. A graded mesh refinement approach for boundary layer originated singularly perturbed time-delayed parabolic convection diffusion problems. Math Methods Appl Sci. 2021;44(16):12332–50.

[7] Shakti D, Mohapatra J, Das P, Vigo-Aguiar J. A moving mesh refinement based optimal accurate uniformly convergent computational method for a parabolic system of boundary layer originated reaction–diffusion problems with arbitrary small diffusion terms. J Comput Appl Math. 2022;404:113167.

[8] Zeinal-Kheiri S, Shotorbani AM, Khardenavis A, Mohammadi-Ivatloo B, Sadiq R, Hewage K. An adaptive real - time energy management system for a renewable energy - based microgrid. IET Renew Power Gener. 2021;15(13):2918–30.

[9] Wang B, Peng X, Zhang L, Su P. Real time power management strategy for an all-electric ship using a predictive control model. IET Gener Transm Distrib. 2022;16(9):1808–21.

[10] Zhang S, Xiang Y, Liu J, Liu J, Yang J, Zhao X, et al. A regulating capacity determination method for pumped storage hydropower to restrain PV generation fluctuations. CSEE J Power Energy Syst. 2022;8(1):304–16.

[11] Fang Y, Zhao S, Du E, Li S, Li Z. Coordinated operation of concentrating solar power plant and wind farm for frequency regulation. J Mod Power Syst Clean Energy. 2021;9(4):751–9.

[12] Zhao X, Hanglin LI. Deep neural network compression algorithm based on hybrid mechanism. J Comput Appl. 2023;43(9):2686–91.

[13] Chen L, Xiong H, Sang X, Yuan C, Li X, Kong Q. An innovative deep neural network–based approach for internal cavity detection of timber columns using percussion sound. Struct Health Monit. 2022;21(3):1251–65.

[14] Chen CY, Lai IC, Wu PY, Wu RB. Optimization and evaluation of multidetector deep neural network for high-accuracy Wi-Fi fingerprint positioning. IEEE Internet Things J. 2022;9(16):15204–14.

[15] Adam ABM, Wang Z, Wan X, Xu Y, Duo B. Energy-efficient power allocation in downlink multi-cell multi-carrier NOMA: Special deep neural network framework. IEEE Trans Cogn Commun Netw. 2022;8(4):1770–83.

[16] Das P, Rana S, Vigo-Aguiar J. Higher order accurate approximations on equidistributed meshes for boundary layer originated mixed type reaction diffusion systems with multiple scale nature. Appl Numer Math. 2020;148:79–97.

[17] Das P. An a posteriori based convergence analysis for a nonlinear singularly perturbed system of delay differential equations on an adaptive mesh. Numer Algorithms. 2019;81(2):465–87.

[18] Das P. Comparison of a priori and a posteriori meshes for singularly perturbed nonlinear parameterized problems. J Comput Appl Math. 2015;290:16–25.

[19] Das P, Vigo-Aguiar J. Parameter uniform optimal order numerical approximation of a class of singularly perturbed system of reaction diffusion problems involving a small perturbation parameter. J Comput Appl Math. 2019;354:533–44.

[20] Saini S, Das P, Kumar S. Parameter uniform higher order numerical treatment for singularly perturbed Robin type parabolic reaction diffusion multiple scale problems with large delay in time. Appl Numer Math. 2024;196:1–21.

[21] Kumar S, Kumar S, Das P. Second-order a priori and a posteriori error estimations for integral boundary value problems of nonlinear singularly perturbed parameterized form. Numer Algorithms. 2024;1–28.

[22] Das P, Rana S. Theoretical prospects of fractional order weakly singular Volterra Integro differential equations and their approximations with convergence analysis. Math Methods Appl Sci. 2021;44(11):9419–40.
[23] Srivastava HM, Nain AK, Vats RK, Das P. A theoretical study of the fractional-order p-Laplacian nonlinear Hadamard type turbulent flow models having the Ulam–Hyers stability. RACSAM. 2023;117(4):160.
[24] Das P, Rana S, Ramos H. On the approximate solutions of a class of fractional order nonlinear Volterra integro-differential initial value problems and boundary value problems of first kind and their convergence analysis. J Comput Appl Math. 2022;404:113116.
[25] Das P, Rana S, Ramos H. A perturbation-based approach for solving fractional-order Volterra–Fredholm integro differential equations and its convergence analysis. Int J Comput Math. 2020;97(10):1994–2014.
[26] Das P, Natesan S. Higher-order parameter uniform convergent schemes for Robin type reaction-diffusion problems using adaptively generated grid. Int J Comput Methods. 2012;9(4):1250052.
[27] Das P. Richardson extrapolation method for singularly perturbed convection-diffusion problems on adaptively generated mesh. CMES. 2013;90(6):463–85.
[28] Das P, Natesan S. A uniformly convergent hybrid scheme for singularly perturbed system of reaction-diffusion Robin type boundary-value problems. J Appl Math Comput. 2013;41:447–71.